Renewable Energy 153 (2020) 601–614

Contents lists available at ScienceDirect

Renewable Energy

journal homepage: www.elsevier.com/locate/renene

The performance of a weir-mounted tidal turbine: Field observations and theoretical modelling

M.C. Verbeek *, R.J. Labeur , W.S.J. Uijttewaal

Department of Hydraulic Engineering, Delft University of Technology, Stevinweg 1, 2628 CN, Delft, the Netherlands

ARTICLE INFO

Article history:
Received 18 April 2019
Received in revised form
13 January 2020
Accepted 2 February 2020
Available online 5 February 2020

Keywords:
Production
Tidal turbines
Field monitoring
Weir
Theoretical model

ABSTRACT

An economical way to harvest tidal energy is by integrating free stream turbines in coastal infrastructure. While numerous studies have investigated how turbines should be arranged in idealized geometries to optimize their performance, only a few have considered the influence of realistic bed features. This research investigates the influence of a hydraulic structure on the performance of a tidal turbine, using the combination of field monitoring of full scale turbines installed in a Dutch storm surge barrier - comprising a weir and pillars - and by developing a corresponding theoretical model.

The observed production by the turbines was large compared to situations with an unconstrained flow for two reasons. Firstly, the flow contraction by the weir increased the mass flux through the rotor plane. Secondly, the turbine suppressed energy losses in the recirculation zone downstream of a weir. The proposed model provides a quantitative estimate of these effects and is validated against field data. The model can be used as a design tool or parametrization of turbines in a large scale shallow water model, providing performance estimates covering a range of turbine-weir configurations. The work contributes to efficiently exploiting tidal energy with turbines in coastal bridges or flood defenses.

1. Introduction

Energy generation using tidal turbines is a promising new technology, which can supply a significant amount of power to countries with tidal coasts. For example the waters around UK's coast have the potential to provide half of the electricity need of the country [1]. The Levelized Cost of Energy of tidal stream is quantified two to five times higher than exploiting other renewable energy sources such as onshore wind in the UK [2]. A cost reduction may be realized by installing turbines in existing coastal infrastructure - such as dams, storm surge barriers or levees - provided their power output is not significantly reduced. In this light, many researchers have investigated how the performance of turbines is affected when changing their configuration in a tidal channel (e.g. Ref. [3]).

Betz [4], Lanchester [5], and Joukowsky [6] provided the basis for performance studies of wind - and tidal energy turbines, by describing the turbine as an inverse propeller which extracts power proportional to the rotor swept area. Betz [4] derived an expression for the maximum fraction of energy that can be extracted from the flow by applying the 1D balances for mass, energy and momentum to a stream tube passing the rotor area. The theoretical maximum power extraction amounts to 16/27 of the undisturbed energy flux through the rotor plane for a turbine placed in an unconstrained flow [4]. Garrett and Cummins [7] demonstrated that this limit can be exceeded if turbines are installed in a channel, as the lateral confinement of the flow by the channel boundaries enforces a larger mass flux through the rotor plane of the turbines. Garrett and Cummins [7] elaborated on the formulation of Betz [4] by adding an energy balance for the flow bypassing the turbines. They found that power output can be optimized by changing the *local blockage*, defined as the ratio of the total turbine area and the channel area.

Theories to assess the performance of turbines in channels generally consider a flat bed only and can therefore not be applied to situations with an abrupt step in the bathymetry, as is the case for a weir. Smeaton et al. [8] discussed how turbine performance is affected by a smooth constriction in a channel, excluding the effects of flow separation and recirculation. For turbines in the wake of a weir however, these turbulence phenomena govern the volume flux of water bypassing the rotor, while also energy losses downstream of the weir may be affected by the presence of the turbines. The coupled effects of separating flow and the turbine's effect on

* Corresponding author.
E-mail addresses: m.c.verbeek@tudelft.nl (M.C. Verbeek), r.j.labeur@tudelft.nl (R.J. Labeur), w.s.j.uijttewaal@tudelft.nl (W.S.J. Uijttewaal).

https://doi.org/10.1016/j.renene.2020.02.005

the flow field will thus determine the turbine's performance.

Many studies have investigated the performance of tidal turbines by using theoretical or numerical modelling. Validation of such models is generally limited as data from turbines operating at full scale is relatively scarce. For this reason, verification of the underlying model assumptions has mainly relied on laboratory experiments which imposes some restrictions deriving from moderate scalability of intricate details of the flow past turbines. Validation of the calculated performance - using measurements from full-scale turbines - would on the other hand warrant the predictive capability of such models rendering them valuable tools to obtain a quick scan of the power potential of a tidal site.

This study extends the 1D model of Garrett and Cummins [9] and Houlsby et al. [10] to tidal channels with a locally non-flat bed in order to assess the performance of turbines mounted in a hydraulic structure or a weir. Data from a monitoring program of full scale horizontal axis turbines are used to schematize the flow and to verify various other model assumptions. The field data are obtained from turbines installed at the storm surge barrier in the Eastern Scheldt, a tidal estuary in The Netherlands. These observations demonstrate that turbine performance may exceed the theoretical limit, derived by Betz [4], when the turbines are installed nearby a weir. The model can predict an optimal trade-off between energy losses at flood defences and energy harvesting by the turbines.

This paper consists of two parts: (1) field data analyses, and (2), data interpretation through theoretical modelling. In the next section, the methods to acquire the flow - and performance data of the full-scale turbines are discussed and the general modelling concepts are introduced. The field data are presented in the third section for a representative situation during flood and ebb, respectively. These data provide a basis for conceptualization of the flow at a turbine near a weir, where the following two cases are discerned: (1) the turbine is situated downstream of a weir, which at the test site corresponds to flood, and (2), the turbine is situated upstream of a weir, corresponding to the observed ebb tidal stage. The model equations are presented and verified in Section 4, which are used to estimate the turbine thrust coefficient and the fraction of extracted power for different turbine-weir geometries. Conclusions are drawn in Section 5.

2. Methods

2.1. Data acquisition

The hydrodynamics and performance of an array of full-scale turbines is studied in a monitoring programme at a semi-open storm surge barrier in the Eastern Scheldt basin, a tidal estuary in The Netherlands (Fig. 1). The basin is connected to the southern part of the North Sea (Fig. 1a and b). The barrier is a prospective location for harvesting tidal energy, as in principle all gates can be retrofitted with turbines and flow velocity is high. The flow passing the barrier is constrained by both the islands and the bathymetry in the basin mouth, and the pillars and weirs of the barrier Fig. 1c, [11]. The barrier is positioned on top of a submarine sill, which is covered with asphalt mastic and boulders. The structure consists of 62 gates - with an equal amount of weirs - which can be closed during storm surges to protect the hinterland from coastal flooding (Fig. 1c). Since the end of 2015, five horizontal-axis turbines have been installed in the 8th gate of the southern channel.

Each turbine has two blades, a rotor diameter of 5.3 m and an installed capacity of 250 kW. The turbine axes are mounted at a height of −4.83 m NAP (national reference datum) and 6.13 m basin-ward of the gate weir (Fig. 2). The turbine blade tip-to-tip spacing is a quarter rotor diameter. The blade-swept area to channel area ratio amounts to 0.20, with respect to the mean local cross section, and 0.29 with respect to the mean cross-sectional area at the crest of the weir. The turbines are lifted in case the hydraulic head loss over the barrier exceeds 0.6 m during outflow from the basin, or 0.8 m during inflow towards the basin, in order to avoid potentially high structural loading on the barrier and its downstream bed protection. The gauges, which record the corresponding water levels, are located in the approach harbours up- and downstream of the barrier 1 km north of the installation site.

Table 1 summarizes the characteristics of the five sets of data that were obtained in the context of the monitoring: one before the turbines were installed, in 2011, and four after installation of the turbines (Table 1 and Fig. 2). Two- and three beam Teledyne Acoustic Doppler Current Profiler (ADCP) transducers recorded the flow during a spring neap cycle in August 2011. The transducers have a three degree beam angle slanted 20° with respect to the transducer centre line. The transducers were mounted at the gate pillar looking sideways and at the gate sill looking upwards (Fig. 2b). The second and third datasets were recorded with horizontal ADCPs (Signature 1000 [12]) mounted in the turbine hub and strut of the outer and centre turbines (Fig. 2c and d, Fig. 3) with one 16 Hz beam along the mean flow direction. The transducers have an acoustic frequency of 1 MHz and map the flow velocity 25 up- and downstream of the turbines in 50 bins of 0.5 m each. The fourth and fifth datasets are obtained similarly, but with three ADCP beams at 8 Hz.

The flow field at the turbines in dataset 2 to 5 is studied discerning two modes of operation: (1) idle, with the turbines operating at a constant and minimal tip speed relative to the incoming flow velocity at a distance 25 m upstream, taking out no kinetic energy, and (2), loaded, with the turbines operating at a constant and optimal tip speed ratio, extracting energy. The corresponding tip speed ratios are similar for the measured ebb and flood situation. Various variables were recorded for both modes: flow velocity [ms^{-1}] at 8 Hz and 16 Hz, turbine loads [N] at 1 MHz, including the axial thrust force, bending moments [Nm] at 1 MHz, rotational speed at 1 Hz and net production [kWh] at 1 Hz.

2.2. Data processing

The data of dataset 1 (2011) were processed, giving vertical, lateral and streamwise flow velocity profiles. Hereby, isotropy of the flow between the inclined beams is assumed. The data from the turbine transducer beams (datasets 2 to 5) are not combined into a velocity vector in three directions, because the flow in the turbine wake is strongly anisotropic [13]. Here only the component along the mean flow direction is used in the analysis. This component is a consistent approximation of the mean flow velocity as long as the flow direction is not perpendicular to the transducer beam. This holds since the mean flow direction deviates only up to 10° from the turbine rotation axis when the flow enters the basin during flood. The flow velocity in between the turbines is measured with the side-looking ADCP beams (Fig. 3), quantifying the acceleration of the flow bypassing the array and devices when the turbines are positioned close to each other [14].

The data analyses are not limited to the time-averaged flow fields since the flow over the weir is highly turbulent, which is associated with the sharp local velocity gradient. The turbulence characteristics give insight in the shear layer between the wakes and ambient flow and the recovery of velocity deficits. Guerra and Thomson [15] have already proven that reliable turbulence characteristics can be obtained from shallow seas with the ADCP transducer of this study.

The integral turbulence length scale, L [m], representing the size of the turbulence eddies present in the flow, is estimated for each

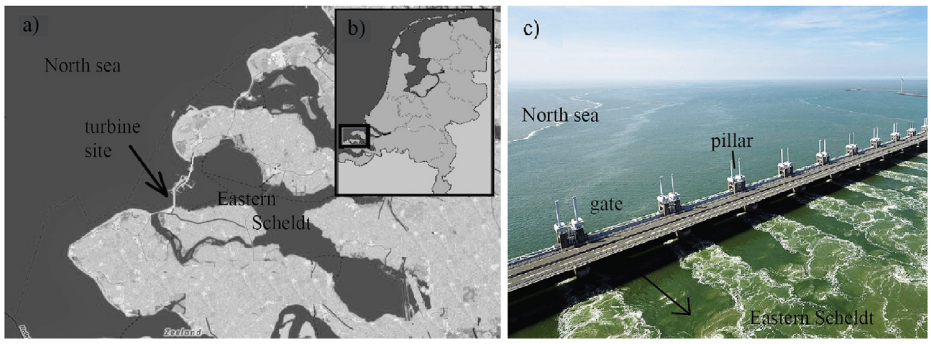

Fig. 1. a) A map of the Eastern Scheldt basin, with the barrier with turbine site indicated with an arrow and b) its location in the Netherlands. c) An aerial photograph of the storm surge barrier and its gates. The arrow indicates the flow direction in one of the gates of the barrier during the flood phase. (source: Rijkswaterstaat).

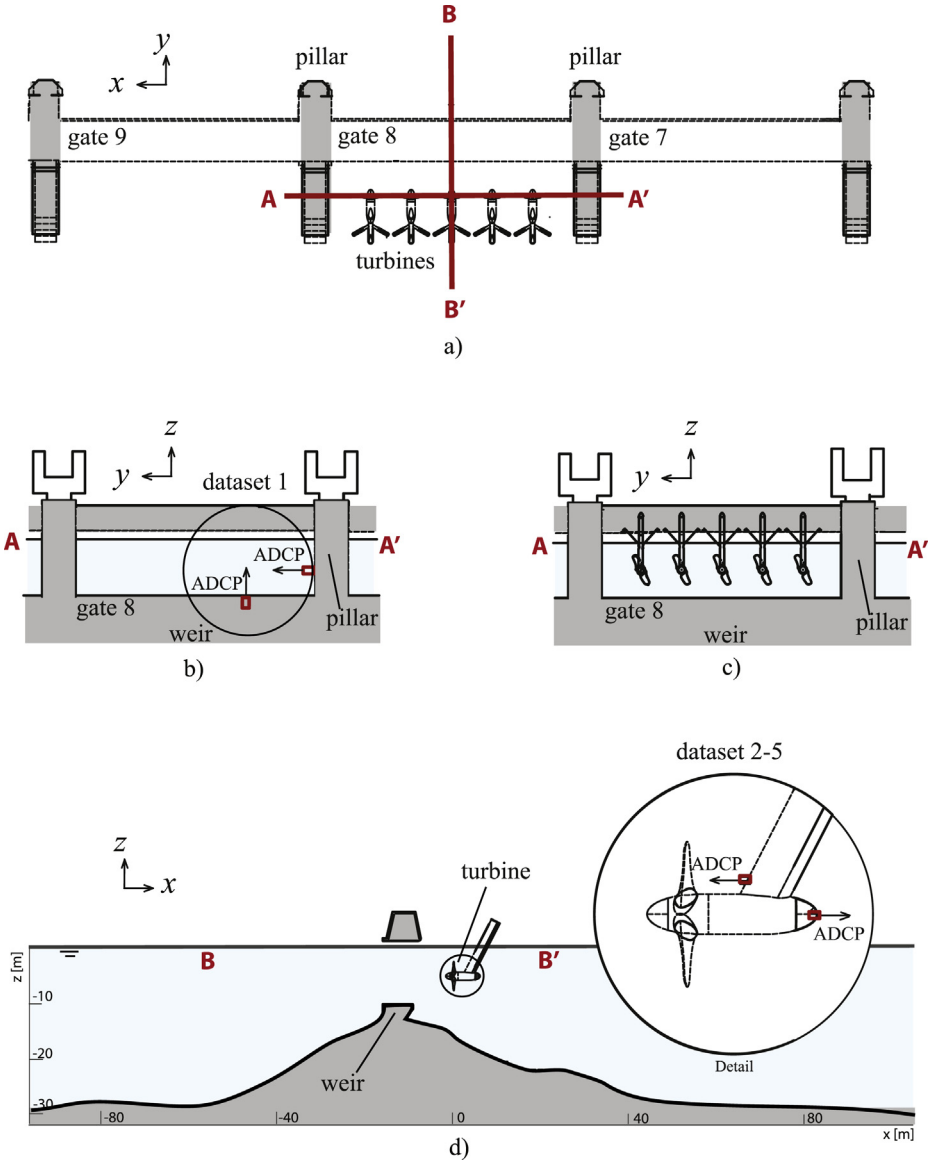

Fig. 2. a) A schematic drawing of the gate with turbines in top-view indicating cross sections A and B (a projection of a 3D view is presented in Fig. 3), b) cross section A showing the gate from the side (looking to the east) with the positions of the two ADCPs mounted during the 2011 survey prior to turbine installation, c) cross section A gives a side view of the turbines to the east, d) cross section B showing the bathymetry over the gate from the side (looking north) and a detail of the turbine with ADCPs.

Table 1
Overview of the characteristics of the five sets of ADCP-data used in the analysis. The exact tip speed ratio (TSR) of the turbines cannot be disclosed. (hor. is horizontal and vert. is vertical.)

Type	Dates	Turbine	ADCP	ADCP	ADCP	ADCP
		Tip speed ratio	Height	Direction	Configuration	Frequency
1	08 16–08 23 2011	No turbine	−9.5 m	vert.	1 device, 3 beams	2 Hz
	08 16–08 23 2011	No turbine	−4.8 m	hor.	1 device, 2 beams	2 Hz
2	10 10 - 10 26 2016	Optimal TSR	−4.8 m	hor.	6 devices, 1 beam	16 Hz
3	08 28–08 29 2017	Minimal TSR	−4.8 m	hor.	6 devices, 1 beam	16 Hz
4	06 20–06 22 2017	Optimal TSR	−4.8 m	hor.	6 devices, 3 beams	8 Hz
5	06 01–06 06 2017	Minimal TSR	−4.8 m	hor.	6 devices, 3 beams	8 Hz

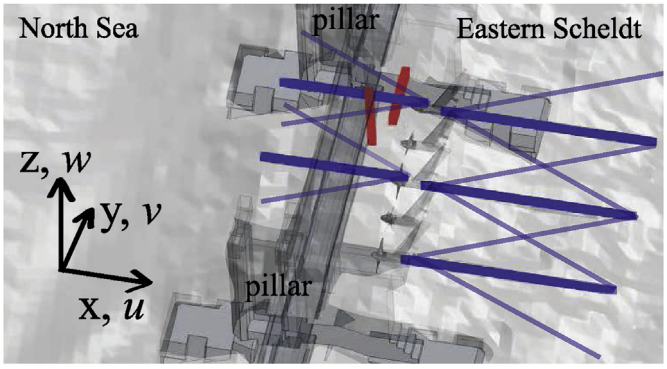

Fig. 3. A 3D view of the turbine array and the ADCP measurement locations of datasets 1 (horizontal and vertical red lines) and 2 to 5 (horizontal blue lines; three per device), x is the direction along the main flow. Courtesy of Deltares. (For interpretation of the references to colour in this figure legend, the reader is referred to the Web version of this article.)

10 min of velocity data. To this end, a turbulence time scale, obtained from a Fourier transformation of the corresponding dataset, is multiplied by the mean velocity, using Taylor's frozen turbulence hypothesis [16], although this is not strictly valid in the wake of the turbine. The method was successfully applied to determine turbulence length scales at an offshore site by Milne et al. [17] and Guerra and Thomson [15]. The turbulence intensity, I [−], which denotes the turbulence level of the flow - or the strength of the velocity fluctuations - is calculated as the ratio between the 10-min averaged root mean square of the turbulent fluctuations and the mean free stream flow velocity measured three rotor diameters (diameter $D = 5.3$ m) upstream of the turbine.

Poor quality data points and data points during the time span of turbine operation outside of the operational tip speed ratio were flagged and filtered out prior to the analysis. These data were excluded based on low signal amplitude, low signal correlation, and the orientation of the ADCP transducers, in line with the work of Milne et al. [18]. The Doppler noise was removed using a low pass filter. The sampling volumes of the seaward-looking transducers were intersected by passing turbine blades two times per blade rotation. The corresponding signal is removed by identifying velocity fluctuations at twice the rotational frequency. Overall, up to 5% of the data obtained during neap tides were removed while 60% of the data obtained during spring tides were removed. This difference is on account of the higher incidence of large water level differences - for which the turbines had to be lifted out of the water - during spring tide. The interpretation of the data will be done through a simple 1D model.

2.3. Model approach

A theoretical model is set up in the second part of this paper. The model aims to quantify how the rotor thrust of a turbine is influenced by a weir, using the 1D balances of mass, momentum and energy. The field data form the basis to schematize the flow fields in the theoretical model, which is validated with thrust data from the turbine in Sec. 3.3. The model approach of Garrett and Cummins [9] is extended with the inclusion of an abrupt step in the bathymetry, representing a weir, for a situation with a turbine upstream of the weir and for a situation with a turbine downstream of the weir. As input the model uses the hydraulic head difference, the deceleration of the flow at the rotor plane, and geometry information, which is in line with the work of Garrett and Cummins [9] and Nishino and Willden [14]. The model may be used as an engineering tool, giving a rapid assessment of both the drag of a barrier and turbine, and the turbine production, which is particularly useful in optimization studies.

3. Data analyses

This section presents the observed hydrodynamics of the flow over a weir at the Eastern Scheldt storm surge barrier, considering representative situations during flood and ebb with the corresponding head differences being defined as positive and negative, respectively. The studied full-scale turbines are located at the lee side of the weir during flood (positive head) and at the upstream side of the weir during ebb (negative head). The turbulence characteristics of the flow are presented in order to interpret the role of the large velocity gradients in the wake flow of the weir, which may converge the flow at the turbine location. This possibly affects turbine blockage and performance. Furthermore, the analysis of turbulence quantities enables a distinction between the respective contributions of the turbine and gate to the flow field, which is relevant to schematize the flow in Sec. 4. The data are shown for a time-averaged head over the weir for both an increasing and decreasing water level head, to capture the influence of the tidal stage on the observed profiles. At the end, the hydrodynamics is linked to the performance of the turbine, by relating the observed turbine thrust to the different conditions.

3.1. Hydrodynamics of the weir

The variations in the flow are mainly governed by the tidal cycle, suggesting that the flow at the weir can be assumed quasi-steady, ignoring inertia effects imposed by the tide. In other words, the time variations in the boundary conditions of the flow are slow relative to the travel time of a fluid particle passing the weir. The flow velocity is largest during flood, with a maximum around 4.5 ± 0.5 ms^{-1}. A slightly lower velocity maximum of 3.8 ± 0.2 ms^{-1} is observed during ebb.

Fig. 4 presents the flow field along a vertical and a lateral transect at the weir, prior to the installation of the turbines (dataset 1). Two transducers measured the flow velocity: one looking upwards from the weir crest at a lateral position of $y = 9.8$ m and one

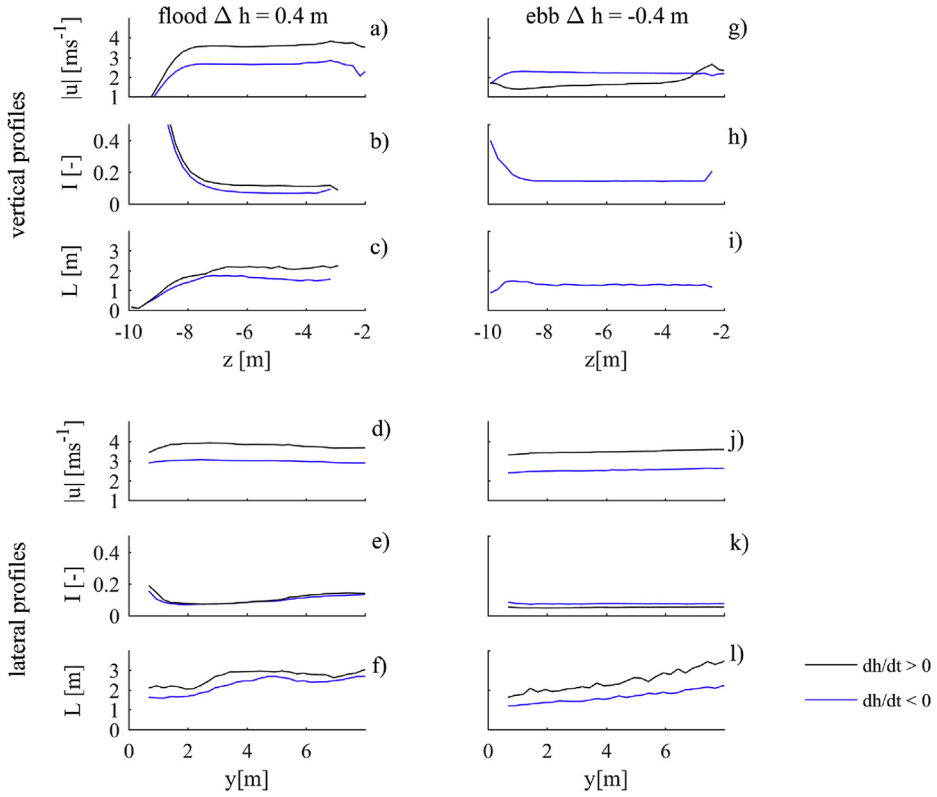

Fig. 4. The time-averaged flow field in a gate without turbines is displayed for a water level head of 0.4 m (panels a–f, flood) and −0.4 m (panels g–l, ebb) over the barrier based on measurements during a spring-neap cycle in 2011 (dataset 1). The pillar is located at a lateral position of $y = 0$ m, the weir crest at a height of $y = -9.5$m. The panels display the vertical (a-c and g-i) and the lateral (d-f and j-l) profiles of the time-averaged streamwise flow velocity u, the streamwise turbulence intensity I, and streamwise turbulence integral length scale L. The dataset is split into conditions for increasing (black) and decreasing (blue) heads. (For interpretation of the references to colour in this figure legend, the reader is referred to the Web version of this article.)

looking sideways from the pillar at a height of z = -4.8 m NAP (Fig. 3). The water surface in Fig. 4a–c and 4g-i is located at approximately a height of $z = 0$ m NAP. The full width of the weir is 39.5 m, of which 8 m is presented in the lateral profiles of Fig. 4d–f and 4j-l.

Fig. 4a–c shows the vertical velocity profile at the weir for the flood situation. The along-stream flow velocity is nearly uniform above a depth of -7.5 m NAP. Variations in the velocity, turbulence intensity and integral length scale are only manifest below this depth. Fig. 4g–i shows the vertical velocity profile for the ebb situation, which is uniform above a depth of $z =$ m NAP. The flow velocity is lower in the ebb situation than in the flood situation. The turbulence intensity has a peak value, namely above 0.2, close to the crest of the weir (z = -9.5 m). The lateral velocity profiles, which are presented in Fig. 4d-f and j-l, are uniform during both the and ebb and flood situation, except from the small peak in turbulence intensity of 0.2 near the pillar (Fig. 4e).

The observations indicate that the flow through the gate is mainly affected by the vertical confinement imposed by the weir. The vertical profile shows a marked decrease in the along-stream velocity close to the crest of the weir, while the flow is largely uniform in the remainder of the profile. The high turbulence intensity near the weir crest indicates that turbulent mixing takes place. The bed level decreases abruptly at the lee side of the weir. Likely, the flow separates downstream of the weir and a recirculation zone develops.

Dataset 3 gives insight in the flow over the weir at a height of 4 m below NAP, that is 5.5 m above the weir crest (Fig. 5b and f). The longitudinal flow velocity at this depth accelerates from 1.5 to 2.0 ms^{-1} to 3.0–3.5 ms^{-1}, over a distance from 10 to 25 m upstream of the weir to the weir crest. Fig. 5c shows that the streamwise turbulence intensity of the flow is highest at the lee side of the weir, namely around 0.2. Here, the turbulence integral length scale increases with the downstream distance from the weir from 2 m to approximately 7 m during flood and from 0.5 m to 3 m during ebb (Fig. 5d and h). These observations are consistent with the flow field obtained from dataset 1 (pre-installation).

The data suggests that the weir confines the flow vertically (dataset 1), hence the flow accelerates when passing the weir (dataset 3). The flow recirculation downstream of the weir, might cause the observed high values in turbulence intensity and integral turbulence length scale at the lee side of the weir when the turbines do not operate. The turbulence integral length scales, and hence the turbulence eddies in the recirculation zone, are possibly larger at larger distances from the weir where the water depth increases. The influence of inertia on the main flow characteristics, judged from the difference between the blue and black lines in the figures, is limited, though slightly larger during flood when the flow velocity is largest.

3.2. Hydrodynamics of the weir with turbines

The flow field at the weir changes significantly when the turbines are loaded. The differences with the flow field when the turbines are in idling mode are presented in Fig. 6. The along-stream flow velocity in the centre line of the turbine axis decreases when the turbine extracts energy. This results in a small velocity deficit one rotor diameter upstream of the turbine and a velocity deficit equal to half

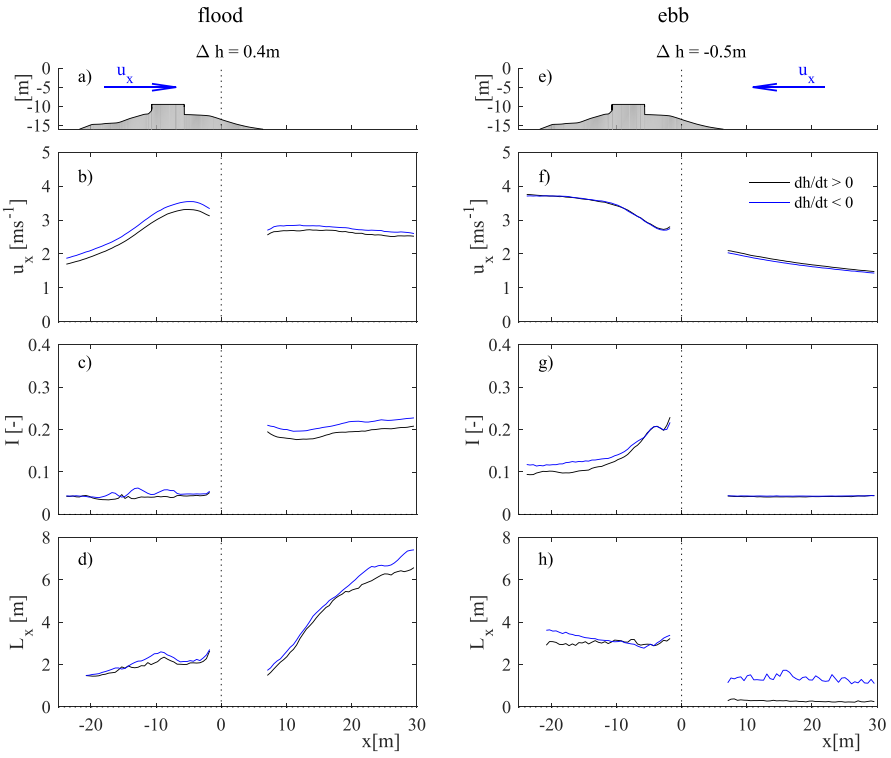

Fig. 5. The streamwise flow field at the weir at a water depth of approximately −4 m, that is 5.5 m above the weir crest, at the centre of the weir for a water level difference of 0.4 m (a–d) and −0.5 m (e–h). The flow field is obtained, with turbines in idling mode (dataset 3). The panels present a longitudinal transect of the bathymetry over the weir (a,e) and the corresponding along-stream profiles of the flow velocity (b,f), the streamwise turbulence intensity (c,g), and the turbulence integral length scale (d,h). The dataset is split into conditions for increasing (black) and decreasing (blue) heads. (For interpretation of the references to colour in this figure legend, the reader is referred to the Web version of this article.)

of the undisturbed velocity in the turbine wake (Fig. 6b,f). The velocity deficit is largest at a distance of 2*D* downstream of the turbine during flood and at a distance of 0.5*D* downstream of the turbine during ebb. The ebb wake is rather short and the deceleration mainly occurs upstream of the rotor plane. Possibly, the contraction of the ambient flow at the weir enhanced turbulent mixing and hence the recovery of the ebb wake.

The turbulence intensity did only increase with 0.05 or 0.1 with respect to a situation with the turbines in idling mode (Fig. 6c,g). This suggests that most of the observed turbulent fluctuations originate from the ambient flow over the weir, rather than from the turbines. The integral turbulence length scale decreases by 2 m in the turbine wake (Fig. 6d,h). The latter may be a consequence of the flow bypassing the turbine along the bed, which is suppressing the height of the recirculation zone downstream of the weir (Fig. 8). This suggests that energy, otherwise lost in turbulence, becomes available to the energy harvesting by the turbine.

Fig. 7 depicts the turbine-induced changes to the flow in a horizontal plane at approximately the axis height of the turbines. To this end, the flow field for turbines in idling mode is subtracted from the flow field with the turbines loaded. The data is measured with the transducers at the turbines as presented in Fig. 3.

There is a velocity deficit downstream of the turbines, in the wakes, while there is a velocity surplus in the area in-between the turbines and their wakes, the so-called bypass area (Fig. 7a). The increase of the flow velocity in the bypass area amounts to 0.2 ms^{-1} relative to an ambient velocity of 2.0 ms^{-1} at a head difference of 0.3 m. The relative velocity increase in the bypass was approximately the same for other analyzed water level heads over the barrier up to 0.5 m. The acceleration of the bypass flow was less distinct during the ebb phase (Fig. 7b).

The flow may accelerate in the bypass area if the turbine swept area comprises a considerable fraction of the total channel area [9]. The turbine performance is then likely affected by local blockage, which increases the mass flux through the rotor. The observed increase of the flow velocity adjacent to the wakes suggests that local blockage affects performance of the turbines at the weir. The local blockage is larger during the flood phase (Fig. 8a), than during the ebb phase (Fig. 8b), which is attributed to the weir and its downstream recirculation zone that vertically converge the flow at the turbine location during flood.

3.3. Turbine thrust

Fig. 9 presents the observed thrust force *T* on the turbine for the ebb and flood situation, normalized by a theoretical thrust, using

$$T / T_0 = T / (\rho \Delta h g A_D), \quad (1)$$

where ρ is the water density, A_D is the rotor swept area (22.1 m^2), and Δh is the available head at the weir. This thrust ratio is higher during flood than during ebb for the same water level head, which implies that either the ambient flow velocity or the thrust coefficient of the turbine or both are higher for the flood situation. The standard deviation of the ratio appears larger at a head difference around 0.2 m, which may be a processing artefact. When the local flow velocity reached the cut-in speed of the turbines around this head, the filtering routine could not discern all data from accelerating or decelerating turbine conditions.

The value of the thrust ratio is likely dependent on the geometry only, judging from the fact that similar values are found for different instants during ebb and flood, respectively. The observed

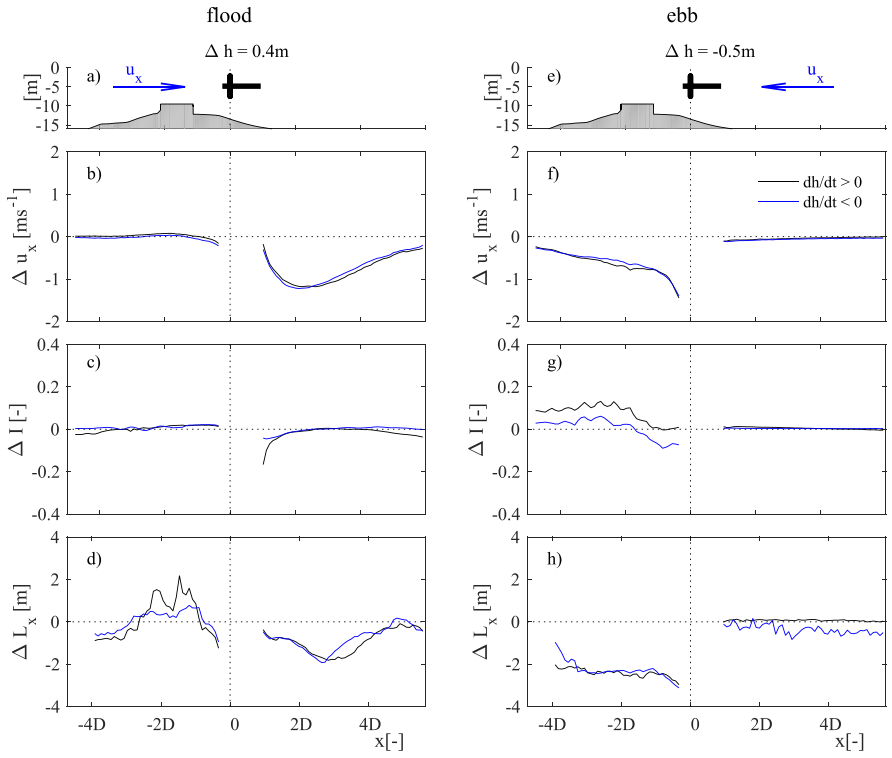

Fig. 6. The streamwise flow field at the weir at a water depth of approximately −4 m (axis height) for the centre turbine of the array for a water level difference of 0.4 m (a–d) and −0.5 m (e–h) presented as the difference (a deficit) between a turbine in idling mode (dataset 3) and a turbine loaded (dataset 2). The panels display a cross section of the bathymetry over the weir with turbine (a,e) and the corresponding along-stream profiles of the flow velocity deficit (b,f), the turbulence intensity deficit (c,g), and the turbulence integral length scale deficit (d,h). The dataset is split into conditions for increasing (black) and decreasing (blue) heads. The horizontal axis is normalized by the rotor diameter *D* of 5.3 m. (For interpretation of the references to colour in this figure legend, the reader is referred to the Web version of this article.)

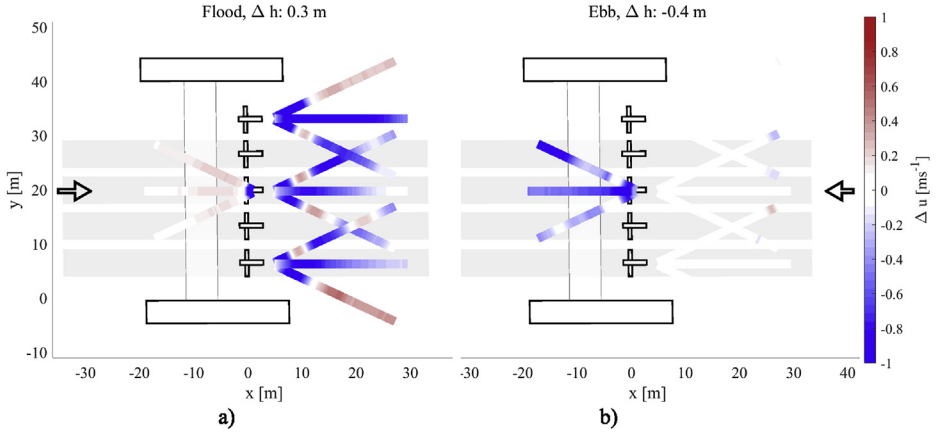

Fig. 7. A top view of the differential flow field at turbine axis height for a head of 0.3 m during flood a), and −0.4 m during ebb b). The panels display the time-averaged flow velocity when the turbines are loaded minus the flow field when they operate in idling mode (dataset 4 and 5). The flow direction is indicated with the black arrow.

thrust ratio slightly decreases for an increasing head during flood which is probably caused by the increase in water depth at the weir. The difference between the ratios for ebb and flood is attributed to the differences in geometry corresponding to each stage. The turbine shape is having a limited contribution to the difference between ebb and flood as it is symmetric.

Garrett and Cummins [9] postulated how the turbine performance in a rectangular channel with two full-slip rigid lid boundaries is affected by the local blockage. Fig. 9 shows the maximum thrust ratio based on the theory of Garrett and Cummins [9], where the blockage is defined as the blade-swept area relative to the conveyance cross section at the weir for the flood situation (giving a blockage of 0.29), and equal to the local channel area at the rotor plane for the ebb situation (0.20). The observed thrust ratio is smaller than the corresponding theoretical value. One of the reasons may be that water can bypass to other gates neighbouring the weir with turbines. However, also the flow separation and expansion downstream of the weir are not included the model schematization of Garrett and Cummins [9].

The next section aims to quantify how rotor thrust is influenced by the weir geometry, by extending the model of Garrett and Cummins [9]. Based on the data analyses, two geometrical

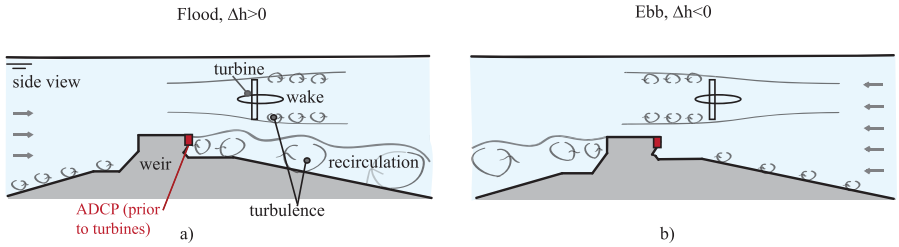

Fig. 8. Impression of the flow passing the weir and the centre turbine of the installation (in side view); the flow recirculates downstream of the lee side of the weir (indicated with instantaneous turbulence rollers in the flow). The turbine is situated at the lee side of the weir during flood a) ($\Delta h > 0$), and at the leading side of the weir during ebb b) ($\Delta h < 0$). The upward looking ADCP transducer, which measured the flow field prior to installing the turbines in 2011 is indicated in red. (For interpretation of the references to colour in this figure legend, the reader is referred to the Web version of this article.)

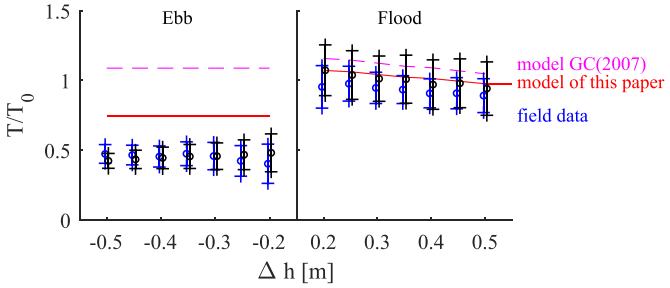

Fig. 9. A series of box plots of the mean observed thrust ratio T/T_0 as defined in Eq. 1 ($\circ$) and its standard deviation ($+$) of the centre turbine of the array at different tidal stages, where the dataset is split into conditions for increasing (black) and decreasing (blue) heads. The quantity on the horizontal axis, Δh, is the water level head over the weir; at positive head (flood), the turbine is downstream of the weir. The lines show the thrust ratio calculated with two models using a set of input variables discussed in Appendix C. (For interpretation of the references to colour in this figure legend, the reader is referred to the Web version of this article.)

parameters can be identified having an additional influence on the turbine thrust at a weir, besides the lateral confinement of the flow in a rectangular channel. The first parameter is the size of the recirculation zone downstream of the weir, as the energy is dissipated in the expansion of the flow downstream of the weir. The second parameter is the vertical confinement or blockage by the weir. While the recirculation is indirectly of importance, affecting mainly the downstream flow field, the local blockage directly increases the local velocity, augmenting the mass flux through the turbine.

4. Modelling turbine performance at a weir

In this section a theoretical model is proposed that accounts for the influence of a weir on turbine performance in a single gate or channel. In line with the work of Garrett and Cummins [9] we use a simplified representation of the flow based on the 1D balance equations for mass, momentum and energy. The field study indicated that this approximation can be made as the flow fields observed in the rotor swept area and the bypass, respectively, were largely uniform which also motivates the use of a bulk thrust ratio for the entire rotor plane. Furthermore, the quasi-steady approximation is made since the measured turbine thrust is controlled by stationary processes such as the wake deceleration, bypass acceleration and turbine thrust ratio which were all similar for different tidal stages.

The horizontal-axis turbine is represented by a so-called actuator disk, assuming an homogeneous distribution of the blade influence over the disk and neglecting angular momentum of the flow. The bed is assumed horizontal while the weir is schematized with a horizontal crest, a vertical trailing edge, and a streamlined leading edge. The flow in the channel is schematized via two streamtubes and a recirculation zone. One streamtube passes the disk (indicated D) while the other one follows the bypass (indicated B) (Figs. 10 and 11). The latter comprises the flow bypassing the rotor at the upper, lower and lateral sides. The recirculation zone extends along the bed between the flow detachment point at the downstream end of the weir and the reattachment point in the far wake of the turbine. The flow velocity in this zone is assumed to have a negligible magnitude, in accordance with the field observations. The presence of the step in the bed with a recirculation zone downstream of it distinguishes this schematization from the one used in the model of Garrett and Cummins [9].

The water passing the weir and turbines is considered an ideal fluid: incompressible, inviscid, and with a constant density. The flow in the model domain is assumed to be steady and normal to the weir and the streamlines are supposed to have a limited curvature only. Owing to the latter, the streamwise pressure gradient is constant within each cross section of a streamtube which - in the absence of shear stress and streamline curvature - leads to laterally uniform velocity distributions in each streamtube. Consistent with this approximation, it is assumed that neither momentum nor energy is transferred between the streamtubes.

The free surface is approximated using a free-slip rigid lid, hence the model is valid for flows with small Froude numbers only. The local variation of the free surface level is then negligible relative to the flow depth. The rigid lid position is based on the water level at the turbine which can vary during the tidal cycle. The flow velocity at the inflow - and outflow boundary (stations 1 and 7, respectively) is assumed to be uniformly distributed and equal in magnitude, as a consequence of the horizontal bottom and free surface. The respective velocities within the domain are expressed as a factor times the inflow velocity u_1 (at station 1), using the velocity factors α in the turbine streamtube and β in the bypass. The velocity factor corresponding to station 2, α_2, is defined as the ratio between velocity at station 2 and 1: $\alpha_2 = u_2/u_1$. The velocity factors of the station 3 to 6 are defined relative to the velocity at station 2 at the weir crest; e.g. the velocity factor at station 3 in the rotor plane is defined as $\alpha_3 = u_{3D}/u_2$. All velocities within the domain are summarized in Fig. 10 and Table 2.

The resulting non-dimensional flow problem is solved when the cross sections of the streamtubes at every station along the channel are known. Additionally, the dimensional problem is solved when the corresponding pressure and velocity distributions are known. The velocity factor at the disk α_3, the weir area relative to the cross section above the weir a, the rotor swept area relative to the cross section above the weir, i.e. the local blockage $1/R$, and the pressure difference between stations 1 and 7, are supposed to be known. Hence, the velocity factors α_5, β_3, β_5 and the undisturbed velocity u_1 are the remaining unknowns. Therefore, to solve the algebraic problem, four equations need to be formulated. These include a

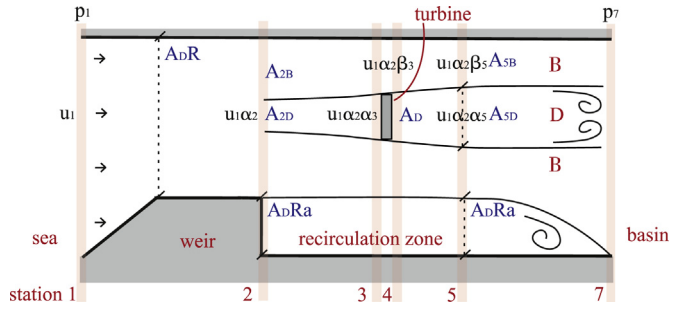

Fig. 10. A schematic sketch of the flood flow via a streamtube passing the turbine (indicated *D*), a bypass streamtube (indicated *B*), and a recirculation zone of the weir. The numbers refer to the stations of the model schematization. The respective velocities within the domain are expressed as a factor times the inflow velocity u_1 (at station 1), using the velocity factors α in the turbine streamtube and β in the bypass. The cross-sectional area of a streamtube at each station is expressed as the product of the rotor-swept area A_D, the relative weir area a, and the blockage $1/R$. An overview of the velocity and cross section of each streamtube is given in Table 2.

Table 2
Definitions of the streamtube cross sections and corresponding flow velocities at stations n for the flood situation; A_{nB} is the cross section of the bypass streamtube, A_{nD} is the cross section of the streamtube passing the turbine, and A_n is the cross section of the entire channel including the recirculation zone (See also Fig. 10 for the corresponding schematization of the flow.).

n	1, 7	2	3, 4	5
A_{nB}	–	$A_D(R-\alpha_3)$	$A_D(R-1)$	$A_D(R-\alpha_3/\alpha_5)$
A_{nD}	–	$A_D\alpha_3$	A_D	$A_D\alpha_3/\alpha_5$
A_n	$A_DR(1+a)$	A_DR	$A_DR(1+a)$	$A_DR(1+a)$
u_{nB}	–	$u_1\alpha_2$	$u_1\alpha_2\beta_3$	$u_1\alpha_2\beta_5$
u_{nD}	–	$u_1\alpha_2$	$u_1\alpha_2\alpha_3$	$u_1\alpha_2\alpha_5$
u_n	u_1	–	–	–

mass balance between stations 1 and 2, two mass balances for the streamtubes *B* and *D*, respectively, and a balance for horizontal momentum between the start and end of streamtube *D*. The position of this streamtube relative to the weir differs for the flood and ebb situation, hence two different schematizations are required which is discussed below. The solution procedures for the resulting systems of equations are presented in Appendices A and B.

4.1. Model for the flood situation

The schematized flood situation has the disk positioned one rotor diameter downstream of the weir, which is in accordance with the geometry of the field situation (Fig. 10). Table 2 gives the cross sectional areas of the streamtubes at the respective stations, where A_D denotes the turbine area, A_DR the channel cross section at the crest of the weir, and R the ratio between the channel cross section and the rotor-swept area, also referred to as the inverse of the blockage [−] [9]. The frontal area of the weir relative to the channel cross section at the crest of the weir is denoted a [−].

4.1.1. Mass balances

Mass is conserved in the channel between stations 1 and 2 which, using a constant density, results in

$$Q = A_1u_1 = A_2u_1\alpha_2, \tag{2}$$

in which Q denotes the discharge in the channel [m^3s^{-1}], α_2 is the flow velocity factor at station 2 [-], u_1 is the inflow velocity [ms^{-1}] at station 1, and A_n is the channel cross section as defined in Table 2. Likewise, equating the mass fluxes in stations 2 to 5 of the streamtube *B* (bypass) results in Ref. [9].

$$Q_B = u_1\alpha_2A_{2B} = u_1\alpha_2\beta_3A_{3B} = u_1\alpha_2\beta_5A_{5B}, \tag{3}$$

where Q_B denotes the discharge in streamtube *B* [m^3s^{-1}]. Similarly, the mass balance for streamtube *D* (turbine) gives

$$Q_D = u_1\alpha_2A_{2D} = u_1\alpha_2\alpha_3A_{3D} = u_1\alpha_2\alpha_5A_{5D}, \tag{4}$$

in which Q_D denotes the discharge in streamtube *D*, where it is noted that $Q = Q_B + Q_D$.

4.1.2. Energy balances

The energy balance equations for the channel between stations 1 and 2, and for the streamtubes *B* and *D* between stations 2 and 5, involve the pressure distributions in stations 2, 4 and 5, respectively. These pressure distributions are needed later on to close a balance for horizontal momentum between stations 2 and 5. Pressure is defined with respect to the hydrostatic states, as the governing equations involve pressure differences due to the dynamics only.

The flow contracts smoothly, with negligible energy dissipation, between stations 1 and 2 resulting in a constant energy head H [m] along this section, which is given by

$$H = u_1^2/(2g) + p_1/(\rho g) = u_1^2\alpha_2^2/(2g) + p_2/(\rho g), \tag{5}$$

where g is the gravitational acceleration [ms^{-2}], ρ is the density of water [kgm^{-3}], and p_n [$kgms^{-2}$] is pressure at station n.

The energy head H_B in streamtube *B* is also approximately constant between stations 2 and 5, due to the weak curvature of the streamlines, which leads to

$$\begin{aligned} H_B &= u_1^2\alpha_2^2/(2g) + p_2/(\rho g) = u_1^2\alpha_2^2\beta_3^2/(2g) + p_{3B}/(\rho g) \\ &= u_1^2\alpha_2^2\beta_5^2/(2g) + p_5/(\rho g). \end{aligned} \tag{6}$$

Using similar arguments, the energy head in streamtube *D* can be assumed piecewise constant - with a discontinuity at the disk - discerning the energy head upstream of the turbine H_{3D}, between stations 2 and 3,

$$H_{3D} = u_1^2\alpha_2^2/(2g) + p_2/(\rho g) = u_1^2\alpha_2^2\alpha_3^2/(2g) + p_{3D}/(\rho g), \tag{7}$$

and the energy head downstream of the turbine H_{4D}, between stations 4 and 5,

$$H_{4D} = u_1^2\alpha_2^2\alpha_3^2/(2g) + p_{4D}/(\rho g) = u_1^2\alpha_2^2\alpha_5^2/(2g) + p_5/(\rho g), \tag{8}$$

in which p_{3D} and p_{4D} denote the pressure in streamtube *D* upstream and downstream of the turbine disk, respectively.

4.1.3. Momentum balance

Applying the balance equations for horizontal momentum to the channel section between stations 2 and 5 leads to

$$\begin{aligned} &Qu_1\alpha_2 + A_2p_2/\rho) - F_w/\rho - F_t/\rho \\ &\quad = Q_Bu_1\alpha_2\beta_5 + Q_Du_1\alpha_2\alpha_5 + A_{5p5}/\rho \end{aligned} \tag{9}$$

in which F_w is drag force on the trailing edge of the weir and F_t is the turbine thrust.

Starting with the latter, the turbine thrust is formulated using

$$F_t = \rho u_1^2 C_T A_D / 2, \tag{10}$$

in which C_T [−] is the thrust coefficient. The thrust results from the net pressure force on the disk [4,19], which is given by the product of the disk area and the pressure difference between stations 3 and 4 of streamtube *D*. Therefore, the thrust coefficient C_T [−] can be defined alternatively by combining equations (6)–(8), giving

$$C_T = (p_{3D} - p_{4D}) \Big/ \left(1 \Big/ 2\rho u_1^2\right) = \alpha_2^2\left(\beta_5^2 - \alpha_5^2\right), \tag{11}$$

which coincides with the definition of Eq. (1) of T/T_0 *if* $u_1^2/2 = \Delta hg$. The resulting power coefficient C_P, used later on, is simply obtained by multiplying C_T with the local velocity factor $\alpha_2\alpha_3$.

Finally, to close equation (9), the drag force F_w on the trailing edge of the weir is formulated. To this end, the pressure distribution in cross section 2 is assumed to be hydrostatic which is a valid approximation as the local streamlines are nearly parallel and the flow velocity in the recirculation zone is relatively small, see Fig. 10. The drag force F_w is then given by

$$F_w = -p_2 R A_D a. \tag{12}$$

4.2. Model for the ebb situation

Fig. 11 shows the flow schematization for the ebb situation with the turbine positioned just upstream of the leading edge of the weir. A few rotor diameters upstream from the turbine the flow is undisturbed (station 2). The wake downstream of the turbine has expanded before it reaches the crest of the weir, leading to parallel streamlines at station 5, while it has largely recovered at the end of the weir (station 6). This reflects the field observations of the velocity deficit during ebb.

The required mass and energy balances are largely similar to those used in the flood model (Eqs. (3) and (4) and (6)–(8)), but the conveyance areas and velocities need to be redefined before applying these equations to the ebb configuration. For convenience, the equations are reformulated below using the modified parameters listed in Table 3. Importantly, the relative velocity α_2 equals 1, because the flow velocity at station 2 of the ebb model is vertically uniform and equal to the velocity in station 1.

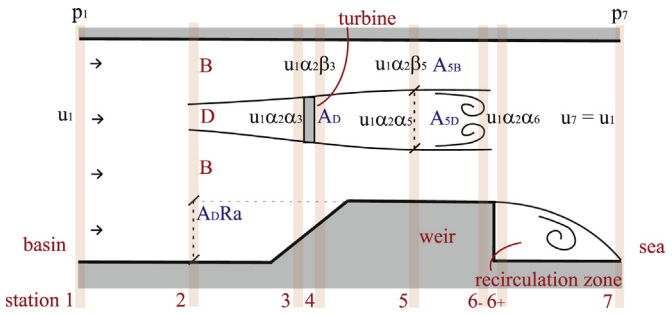

Fig. 11. A schematic sketch of the ebb flow via a streamtube passing the turbine (indicated *D*), a bypass streamtube (indicated *B*), and a recirculation zone of the weir. The numbers refer to the stations of the model schematization. The respective velocities within the domain are expressed as a factor times the inflow velocity u_1 (at station 1), which is equal to the velocity at station 2, using the velocity factors α in the turbine streamtube and β in the bypass. The cross-sectional area of a streamtube at each station is expressed as the product of the rotor-swept area A_D, the relative weir area *a*, and the blockage $1/R$. An overview of the velocity and cross section of each streamtube is given in Table 3.

4.2.1. Mass balances

Equating the discharge in streamtube *B* at stations 2, 3 and 5 gives

$$Q_B = u_1 A_{2B} = u_1 \beta_3 A_{3B} = u_1 \beta_5 A_{5B}. \tag{13}$$

Similarly, the constant discharge in streamtube *D* leads to

$$Q_D = u_1 A_{2D} = u_1 \alpha_3 A_{3D} = u_1 \alpha_5 A_{5D}. \tag{14}$$

4.2.2. Energy balances

Assuming a sufficiently smooth contraction of the bypass, the energy head [m] in streamtube *B* at stations 2, 3 and 5 are equated to give

$$\begin{aligned} H_B &= u_1^2 \Big/ (2g) + p_2 \Big/ (\rho g) = u_1^2 \beta_3^2 \Big/ (2g) + p_{3B} \Big/ (\rho g) \\ &= u_1^2 \beta_5^2 \Big/ (2g) + p_5 \Big/ (\rho g). \end{aligned} \tag{15}$$

For streamtube *D*, the energy head upstream of the turbine at stations 2 and 3 is given by

$$H_{3D} = u_1^2 \Big/ (2g) + p_2 \Big/ (\rho g) = u_1^2 \alpha_3^2 \Big/ (2g) + p_{3D} \Big/ (\rho g), \tag{16}$$

while downstream of the turbine, at stations 4 and 5, the energy head is given by

$$H_{4D} = u_1^2 \alpha_3^2 \Big/ (2g) + p_{4D} \Big/ (\rho g) = u_1^2 \alpha_5^2 \Big/ (2g) + p_5 \Big/ (\rho g). \tag{17}$$

4.2.3. Momentum balance

Conservation of horizontal momentum in streamtube *D* between stations 2 and 5 gives

$$Q_D u_1 + A_{2D} p_2/\rho - F_t/\rho + F_l/\rho = Q_D u_1 \alpha_5 + A_{5D} p_5/\rho, \tag{18}$$

in which F_t is the turbine thrust, given by Eq. (10), and F_l is the horizontal component of the external pressure force on the lateral boundary of streamtube *D*. The latter is calculated as the product of the increase in the streamtube area and the average pressure between stations 2 and 5,

$$F_l = (A_{5D} - A_{2D})(p_5 + p_2)/2, \tag{19}$$

which is a reasonable approximation if the expansion of the wake over the weir is small relative to the weir height, which is in line with the field situation. Though, this schematization of the ebb situation has limited, as the weir drag is not explicitly incorporated, it is the best we can think of for now.

4.3. Verification and validation

The set of equations constituting the flood model and ebb model prescribe the streamtube cross sections at the considered stations, the corresponding velocity factors α and β, and the turbine thrust coefficient C_T, as functions of the blockage $1/R$ and the relative weir height *a*. The algebraic solution procedure is explained in Appendices A and B.

It has been verified that the model results converge to the analytical results of Betz [4] for a vanishing blockage ($1/R \to 0$) and vanishing relative weir height ($a \to 0$). In this situation the bypass velocity factors β approach a uniform value of one, while the velocity at the turbine converges to the average of the free stream

Table 3
Definitions of the streamtube cross sections and corresponding flow velocities at stations n for the ebb situation; A_{nB} is the cross section of the bypass streamtube, A_{nD} is the cross section of the streamtube passing the turbine, and A_n is the cross section of the entire channel including the recirculation zone (See also Fig. 11 for the corresponding schematization of the flow.).

n	$1, 2, 7$	$3, 4$	5	6^-	6^+
A_{nB}	$A_D(R + Ra - \alpha_3)$	$A_D(R + 1/2Ra - 1)$	$A_D(R - \alpha_3/\alpha_5)$	–	–
A_{nD}	$A_D\alpha_3$	A_D	$A_D\alpha_3/\alpha_5$	–	–
A_n	$A_DR(1 + a)$	$A_DR(1 + 1/2a)$	A_DR	A_DR	$A_DR(1 + a)$
u_{nB}	–	$u_1\alpha_2\beta_3$	$u_1\alpha_2\beta_5$	–	–
u_{nD}	–	$u_1\alpha_2\alpha_3$	$u_1\alpha_2\alpha_5$	–	–
u_n	u_1	–	–	$u_1\alpha_2\alpha_6$	$u_1\alpha_2\alpha_6$

velocity and the velocity in the wake of the turbine, $\alpha_3 = 1/2(1 + \alpha_5)$. Furthermore, it has been verified that for arbitrary blockage $1/R$ and vanishing relative weir height a the results converge to those obtained with the model of Garrett and Cummins [9].

Next, the model is validated against the field data using blockage and relative weir height from the observed ebb and flood conditions (see Appendix C). The tidal water level at the weir varies in time. Using the rigid lid approximation, the position of the free surface in the model is varied accordingly. A validation of the calculated thrust coefficients is presented in Fig. 9. The calculated thrust coefficients of the flood model fit nicely within the measured range, suggesting that the most important processes influencing the turbine thrust are included. The model predicts thrust coefficients that are higher than those derived from the field observations for the ebb situation, as the current schematization may overestimate the expansion of the wake over the weir, resulting in a higher thrust. Also, the model does not include the effect of the flow bypassing to neighbouring gates. The observed and predicted thrust coefficients in Fig. 9 vary with the head, in particular during flood. This is attributed to the tidal water level variation at the turbine, an effect that is reproduced reasonably well by the model.

The model excludes free surface phenomena, besides the water level variation at the turbine due to the tide. The rapid, local variations of the free surface level relative to the water depth scale with the square of the Froude number, which is small for the Froude numbers observed in the field that never exceeded 0.5. Although this justifies the use of a rigid lid, a free surface approximation such as postulated by Whelan et al. [20], Houlsby et al. [10], or Vogel et al. [21], would be a useful extension to the model when applying it to relatively higher steps in the bathymetry which are associated with higher Froude numbers.

4.4. Performance estimate

The performance of the weir-mounted turbine can be quantified with the power coefficient,

$$C_P = \alpha_2\alpha_3 C_T, \tag{20}$$

which gives the fraction of the energy extracted by the turbine compared to the energy available in the flow through to rotor swept area in absence of the turbine. Here, $\alpha_2\alpha_3$ is the velocity factor at the turbine disk and C_T is the turbine thrust coefficient.

However, our main interest is to determine the weir-turbine configuration for which the production is maximal for a given head Δh, hence an additional non-dimensional number is introduced to compare the produced power to the nominal power. The nominal power, P_0, can be defined as the energy available in the flow in the channel, A_DR, driven by the head difference Δh,

$$P_0 = u_1\rho g\Delta h A_D R, \tag{21}$$

where Δh is the available head at the weir [m] and g is the gravitational acceleration [ms^{-2}]. Scaling the power P delivered by the turbine with the nominal power P_0 gives the following dimensionless performance measure,

$$\eta = P \Big/ P_0 = C_P u_1^2 \Big/ (2g\Delta hR), \tag{22}$$

which we refer to as the efficiency. Here, C_P is the turbine power coefficient, and u_1 is the undisturbed inflow velocity, which are both calculated by the model.

4.5. Application

The model can be used to calculate how a turbine performs when it is mounted near a weir and how the design can be optimized for a higher production. The control variables of this flow problem include the relative rotor area of the turbine (the blockage), the relative weir area, and the ratio between the flow velocity at the rotor plane and the undisturbed inflow velocity. The resulting turbine performance can be presented with the power coefficient and the efficiency (Eqs. (20) and (22), respectively).

Here, the validated model is applied to the flow past a schematized weir and turbine. The flow is now forced by a fixed water level difference, as in the observed field situation the turbine operation does not affect the available head. The position of the rigid lid, which represents the water level at the turbine, is taken constant for clarity. An optimal efficiency is calculated by varying the relative deceleration in the rotor plane, $\alpha_2\alpha_3$, for different values of the blockage, $1/R$, and the relative weir area, α. The resulting power coefficient, the optimal efficiency and the relative deceleration in the rotor are presented in Fig. 12a and b, c and d, and e and f, respectively.

The power coefficient gives the fraction of the energy flux extracted by the turbine. It is maximal for a high blockage of the turbine, above 0.4 (Fig. 12a and b), and - in the ebb situation - also for a high relative weir area, as the thrust on the rotor is highest in these cases. The power coefficient is minimal for a relative weir area of 0.12 and a blockage of 0.08 in flood situation. Here, the thrust on the rotor is small, as only a small portion of the mass flux passes through the rotor plane. A higher power coefficient can be obtained when reducing the relative velocity in the rotor plane, $\alpha_2\alpha_3$, while increasing the relative weir area (Fig. 12e). Below, the efficiency of the configuration is discussed to give insight in the production relative to the total energy loss, including losses in viscous processes - such as in the turbine wake and in the attachment of the flow to the bed.

The efficiency is highest for a large blockage - above 0.23 - and a relative weir area around 0.08 for the flood situation (Fig. 12c). This efficiency is higher than for a turbine in a flat-bed channel, where the relative weir area is zero. The efficiency of the channel with a turbine downstream of a weir can exceed the efficiency of a flat-bed channel if energy, which is otherwise lost in the turbine wake or

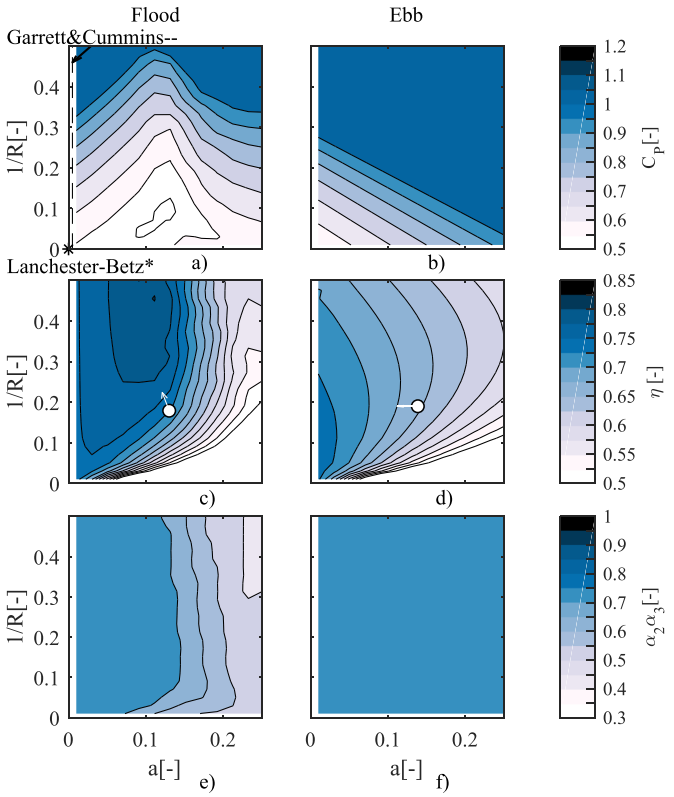

Fig. 12. The estimated power coefficient, C_P, for flood a) and ebb b) conditions for different relative weir areas (horizontal axis) and blockages (vertical axis). The calculated production, P/P_0, for flood b) and ebb c) as defined in Eq. (22). The dot 'o' indicates the geometry of the field situation of which T/T_0 was presented in Fig. 9. The panels e) and f) give the velocity in the rotor plane relative to the undisturbed flow velocity $\alpha_2\alpha_3$ of the model for flood and ebb conditions respectively. The power coefficients as discussed in Garrett and Cummins [9] (– –), and Lanchester [5] and Betz [4] (∗) are indicated in panel a.

recirculation, is used for energy production. This happens when a larger mass flux is forced through the turbine in presence of the weir, than in a flat bed channel. However, this benefit is lost when the relative weir area is further increased and relatively more energy is lost in the turbine wake and recirculation.

An optimum is found for small blockage and small relative weir area in the ebb situation. When increasing the relative weir area and blockage in the model, the flow stagnates and the momentum flux through the rotor decreases. The optimum of the model of the ebb situation did not exceed the efficiency of a turbine in a flat-bed channel.

The difference between the performance for flood and ebb, respectively, can be linked to the mutual roles of momentum advection and the pressure force in transferring power to the rotor blades. In the flood situation, the turbine is situated downstream of the weir and the momentum advected by the flow past the rotor plane is relatively high. In the ebb situation, with the turbine situated upstream of the weir, advection of momentum through the rotor plane is relatively small in favour of the net pressure force on the turbine, as the pressure distribution at the front of the weir is opposite in sign with respect to the flood situation. This difference likely has an effect on the optimal value of the relative velocity in the rotor plane, $\alpha_2\alpha_3$, at which the turbine should be operated to render the production maximal.

For the range of weir-turbine geometries plotted in Fig. 12, the optimal value of $\alpha_2\alpha_3$ varies between 1/3 and 2/ 3 (Fig. 12e and f). While in previous work a value of 2/3 was used to achieve an optimal power coefficient for a turbine in an unconstrained flow or a rectangular channel ([4,5], and [9] respectively), here a smaller value is required to realize an optimal production in some of the considered weir-turbine geometries. A different $\alpha_2\alpha_3$ value may be achieved by changing the turbine design. Vogel et al. [22] already indicated that a turbine with a higher solidity may be required for a constrained flow than for an unconstrained flow to sustain the higher blade forces. The turbine tip speed ratio can also be changed to realize the higher rotor thrust.

The blockage and relative step height of the studied turbines in the Dutch storm surge barrier are indicated in Fig. 12 c and d with a dot. The production of these turbines can be improved by increasing the blockage, moving up in the domain for the flood situation and by decreasing the relative weir area, moving to the left of the calculated domain for the situation during ebb. The production of a weir-mounted turbine could be further optimized by varying the horizontal distance to the weir, which is however not included as a free variable in the present model. Determining the optimal distance of a turbine to a weir will be part of a future study using experimental testing of a weir-mounted tidal turbine.

The data analysis and theoretical modelling confirmed that installation of turbines in a hydraulic structure can be attractive, as the local blockage is high and the energy normally lost in the recovery of a velocity deficit downstream of a weir may become available to energy extraction. The latter is particularly encouraging when the impact of tidal turbines to their installed environment should remain small. The field analysis suggested that the production of a turbine benefits from the installation in a weir, which was largely confirmed by the theoretical model. A hydraulic structure is therefore an attractive location to mount your turbine if no other location providing high blockage is available at the tidal site.

5. Conclusion

This research has extended the 1D turbine performance model of Garrett and Cummins [9] to situations where turbines are installed near a weir or an abrupt expansion of a channel. Data from a monitoring programme at full-scale turbines formed the basis for the modelling. This showed that the weir affected the turbine performance in two ways. Firstly, it increased the local blockage when it was located upstream of the turbine, augmenting the mass flux through the rotor plane. Secondly, the turbine clearly suppressed the dissipation of energy in the recirculation zone downstream of the weir, increasing the extractable fraction of the energy flux of the channel flow. The field data showed that a 1D approach is suited to estimate the performance of full-scale turbines, and the model was verified and validated using the data.

The model provides fundamental insight in the effect of a weir, and particularly of its height, on the performance of a tidal turbine. The extended model serves as a quick design tool or parametrization of turbines in a large scale shallow water model, as it enables the calculation of performance estimates over a range of turbine-weir geometries. The performance could exceed the limit prescribed for turbines in an unbounded channel for specific channel geometries as was demonstrated in previous studies. The paper demonstrates how turbines perform when they are installed in hydraulic structures, revealing the chance to economically exploit energy from tidal currents at bridges and flood defences.

Declaration of competing interests

The authors declare that they have no known competing financial interests or personal relationships that could have appeared to influence the work reported in this paper.

CRediT authorship contribution statement

M.C. Verbeek: Conceptualization, Investigation, Writing - original draft, Visualization. **R.J. Labeur:** Supervision, Writing - review & editing, Funding acquisition. **W.S.J. Uijttewaal:** Supervision.

Acknowledgements

This work was supported by the Netherlands Organisation for Scientific Research within the research programme The New Delta with project number 869.15.008 and the European Regional Development Fund within the project OP-Zuid 2014–2020. We are grateful to Tocardo Solutions B.V. for the use of their velocity and load measurements and to Deltares for the assistance in the data processing.

Appendix A. Solution of the flood model

The proposed model equations can be solved by following the approach described below, defining the head at station 1, $h_1 = p_1/(\rho g)$ [m], to be zero. This pressure at stations 2 and 5, p_2 and p_5 are expressed, using Eqs. (5) and (6):

$$p_2 = 1/2\rho u_1^2\left(1-\alpha_2^2\right), \tag{A.1}$$

$$p_5 = 1/2\rho u_1^2\left(1-\beta_5^2\alpha_2^2\right). \tag{A.2}$$

The expression for the pressures p_2 and p_5 can be substituted in the momentum equation (Eq. (9)). A non-dimensional equation can be derived, using the energy balances given in Eqs. (6)–(8).

$$R\alpha_2^2 + R(1+a)/2\left(1-\alpha_2^2\right) - 1/2\alpha_2^2\left(\beta_5^2-\alpha_5^2\right) - \alpha_2^2\beta_5(R-\alpha_3) - \alpha_2^2\alpha_3\alpha_5 - R(1+a)/2\left(1-\alpha_2^2\beta_5^2\right) = 0. \tag{A.3}$$

Furthermore, Eq. (3) gives the relative bypass velocity at station 3 and 5 [23]:

$$\beta_3 = (R-\alpha_3)/(R-1), \tag{A.4}$$

$$\beta_5 = (R-\alpha_3)/(R-\alpha_3/\alpha_5). \tag{A.5}$$

Lastly, Eq. (2) gives the relative velocity at station 1:

$$\alpha_2 = 1+a. \tag{A.6}$$

Eqs. (A.3) to (A.6) form a closed set of equations solving for the unknowns $\alpha_5, \beta_3, \beta_5$, and α_2, respectively, when of a, R, and α_3 are supposed to be known values.

The momentum balance between stations 5 and 7 is considered,

$$Q_B u_1\alpha_2\beta_5 + Q_D u_1\alpha_2\alpha_5 + A_5 p_5/\rho = A_7\left(u_1^2 + p_7/\rho\right), \tag{A.7}$$

to determine the dimensional velocity u_1 [ms^{-1}]. This equation enables the solution of the dimensional part of the problem for a given head difference between stations 1 and 7.

Appendix B. Solution of ebb model

The relative velocity at station 3 and 4 in the bypass streamtube is defined using Eq. (3), giving:

$$\beta_3 = (R+Ra-\alpha_3)/(R+Ra-1), \tag{B.1}$$

$$\beta_5 = (R+Ra-\alpha_3)/(R-\alpha_3/\alpha_5) \tag{B.2}$$

Using Eq. (18), a non-dimensional momentum balance can be set up between stations 2 and 5, giving:

$$\alpha_3(1-\alpha_5) - \left(\beta_5^2-\alpha_5^2\right)/2 - (\alpha_3+\alpha_3/\alpha_5)\left(1-\beta_5^2\right)/4 = 0, \tag{B.3}$$

in which the head at station 2 is defined to be zero. Eq. (B.1), (B.2), and (B.3) form a closed set to solve for the unknowns β_3, β_5, and α_5, as the values of a, R, and α_3 are assumed to be known values.

The dimensional part of the flow problem can be solved, using a balance of horizontal momentum between station 5 and station 7 given by:

$$Q_B u_1\beta_5 + Q_D u_1\alpha_5 + A_5 p_5/\rho + p_6 aRA_D/\rho = A_7\left(u_1^2 + p_7/\rho\right), \tag{B.4}$$

where aRA_D is the area of the weir in the model. To solve this equation the pressure in station 6 should be known. The pressure distribution between station 6^-, which is located before the weir, and 6^+, which is located after the weir, is assumed to be continuous. The pressure is defined in the horizontal momentum balance between station 5 and 6.

$$Q_B u_1\beta_5 + Q_D u_1\alpha_5 + A_5 p_5/\rho = A_{6^-}\left(u_1^2\alpha_2^2\alpha_6^2 + p_6/\rho\right), \tag{B.5}$$

where α_6 is given, using a mass balance between station 1 and 6 as:

$$\alpha_6 = 1+a. \tag{B.6}$$

The pressure at station 7, p_7, is an input of the model. As a result, the flow velocity u_1 [ms^{-1}] can be calculated.

Appendix C. Input variables for model validation

The modelled thrust ratio's of Fig. 9 required four input values: the relative velocity at the rotor plane, α_3, the blockage, $1/R$, the relative weir height, a and the available head at the structure, Δh. A constant value of $\alpha_3 = 2/3$ is used in the validation, in line with the observations. For the comparison with the model of Garrett and Cummins a relative weir height of 0 is used and for the comparison with model of Betz also a blockage of 0 is modelled. The blockage, $1/R$, and relative weir area, a, are a function of the channel depth, H, and the local water level, h_L, at the weir, as the water level at the weir crest varied over the different tidal stages (Table. C4). The blockage is defined as the rotor swept area divided by the channel area:

$$1/R = A_D/(A_D R) = N(D/2)^2\pi/(HW + h_L W),$$

where A_D is the rotor area with diameter D (5.3 m), N is the number of turbines (5), H is the reference channel depth (9 m), and W is the gate width (39.5 m). The relative weir area is defined as the frontal area of the weir divided by the channel area:

$$a = A_a/(RA_D) = H_a W/(HW + h_L W),$$

where H_a is the height of the weir (4 m).

Table C4
The water level in the gate h_L as a function of the water level head Δh for different tidal stages during the field monitoring.

	Ebb				Flood			
Δh [m]	−0.50	−0.40	−0.30	−0.20	0.20	0.30	0.40	0.50
h_L [m NAP]	−2.00	−2.00	−2.00	−2.00	1.60	1.40	1.10	0.70

It is assumed that 2/3 of the head available at the weir, Δh, is lost in friction before reaching the barrier, in order to compare the model results with the field data.

References

[1] A.S. Bahaj, Generating electricity from the oceans, Renew. Sustain. Energy Rev. 15 (7) (2011) 3399–3416.
[2] A.G.L. Borthwick, Mar. Renew. Energy. Eng. 2 (1) (2016) 69–78, https://doi.org/10.1016/J.ENG.2016.01.011.
[3] R. Vennell, Tuning turbines in a tidal channel, J. Fluid Mech. 663 (2010) 253–267, https://doi.org/10.1017/S0022112010003502.
[4] A. Betz, Das maximum der theoretisch möglichen ausnützung des windes durch windmotoren, Z. für Das. Gesamte. Turbinenwesen Heft 26 (1920). Seiten 307 bis 309.
[5] F. Lanchester, A contribution to the theory of propulsion and the screw propeller, Trans. Inst. Nav. Archit. 57 (1915) 98–116.
[6] N. Joukowsky, Windmill of the Nej Type, Transactions of the Central Institute for Aero-Hydrodynamics of Moscow.
[7] C. Garrett, P. Cummins, The power potential of tidal currents in channels, Proc. Roy. Soc. Lond.: Math. Phys. Eng. Sci. 461 (2060) (2005) 2563–2572, https://doi.org/10.1098/rspa.2005.1494.
[8] M. Smeaton, R. Vennell, A. Harang, The effect of channel constriction on the potential for tidal stream power, Renew. Energy 99 (2016) 45–56, https://doi.org/10.1016/j.renene.2016.06.013.
[9] C. Garrett, P. Cummins, The efficiency of a turbine in a tidal channel, J. Fluid Mech. 588 (2007) 243–251, https://doi.org/10.1017/S0022112007007781.
[10] G. Houlsby, S. Draper, M. Oldfield, Application of Linear Momentum Actuator Disc Theory to Open Channel Flow, OUEL Report 2297/08, Department of Engineering Science, University of Oxford, 2008.
[11] G. Hartsuiker, R. Thabet, J. Dijkzeul, H. Klatter, The Storm Surge Barrier Eastern Scheldt - Evaluation of Water Movement Studies for Design and Construction of the Barrier, Tech. Rep. Z88; PEGESS-N-89011, Delft Hydraulics and Rijkswaterstaat, 8300 AD Emmeloord, 4330 KA Middelburg, The Netherlands, July 1989.
[12] A.S. Nortek, Operations Manual – Signature 250, 500 and 1000, Nortek Group, Red, Norway, 2020. nortekgroup.com/products/signature-1000 (accessed 06 Nov 2018).
[13] P. Schmitt, B. Elsaesser, S. Bischof, R. Starzmann, Field testing of a full-scale tidal turbine part 2: in-line wake effects, in: A.H. Clément (Ed.), 11th European Wave and Tidal Energy Conference, Ecole Centrale Nantes, France, 2015, pp. 1–7.
[14] T. Nishino, R.H.J. Willden, The efficiency of an array of tidal turbines partially blocking a wide channel, J. Fluid Mech. 708 (2012) 596–606, https://doi.org/10.1017/jfm.2012.349.
[15] M. Guerra, J. Thomson, Turbulence measurements from five-beam acoustic Doppler current profilers, J. Atmos. Ocean. Technol. 34 (6) (2017) 1267–1284, https://doi.org/10.1175/JTECH-D-16-0148.1.
[16] F.T.M. Nieuwstadt, B.J. Boersma, J. Westerweel, Turbulence - Introduction to Theory and Applications of Turbulent Flows, Springer International Publishing, 2016, pp. 183–213, https://doi.org/10.1007/978-3-319-31599-7. Ch. Correlation Function and Spectrum.
[17] I. Milne, A. Day, R. Sharma, R. Flay, The characterisation of the hydrodynamic loads on tidal turbines due to turbulence, Renew. Sustain. Energy Rev. 56 (2016) 851–864, https://doi.org/10.1016/j.rser.2015.11.095.
[18] I. Milne, R. Sharma, R. Flay, S. Bickerton, Characteristics of the turbulence in the flow at a tidal stream power site, Phil. Trans. Math. Phys. Eng. Sci. 371 (1985), https://doi.org/10.1098/rsta.2012.0196.
[19] T. Burton, D. Sharpe, N. Jenkins, E. Bossanyi, Aerodynamics of Horizontal-Axis Wind Turbines, Wiley-Blackwell, 2002, pp. 41–172, https://doi.org/10.1002/0470846062.ch3. Ch. 3.
[20] J. Whelan, J. Graham, J. Peiro, A free-surface and blockage correction for tidal turbines, J. Fluid Mech. 624 (2009) 281–291, https://doi.org/10.1017/S0022112009005916.
[21] C. Vogel, G. Houlsby, R. Willden, Effect of free surface deformation on the extractable power of a finite width turbine array, Renew. Energy 88 (2016) 317–324, https://doi.org/10.1016/j.renene.2015.11.050.
[22] C. Vogel, R. Willden, Multi-rotor tidal stream turbine fence performance and operation, Int. J. Mar. Energy. 19 (2017) 198–206, https://doi.org/10.1016/j.ijome.2017.08.005.
[23] T. Nishino, R.H.J. Willden, Two-scale dynamics of flow past a partial cross-stream array of tidal turbines, J. Fluid Mech. 730 (2013) 220–244, https://doi.org/10.1017/jfm.2013.340.